Seasonal to decadal modulation of the impact of El Niño–Southern Oscillation on New Caledonia (SW Pacific) rainfall (1950–2010)

Renaud Barbero[1] and Vincent Moron[1,2,3]

Received 19 July 2011; revised 5 October 2011; accepted 5 October 2011; published 10 December 2011.

[1] New Caledonia (NC; ~166°E, 22°S) rainfall anomalies are more sensitive to central Pacific (CP) El Niño and La Niña events than to those exhibiting highest sea surface temperature (SST) anomalies in the eastern Pacific (EP). The linear relationship between NC rainfall anomalies and CP SST indices peaks from September to March (S–M). The seasonal S–M atmospheric anomalies observed in the South West (SW) Pacific during the warm CP events are highly dissimilar to the EP ones, while there are more similarities during the cold events with a higher amplitude during the CP ones. The warm CP events strengthen the southern Hadley cell around NC longitudes, with positive rainfall anomalies in the equatorial Pacific leading to an anomalous release of latent heat in the upper troposphere and an increased subsidence in the SW Pacific. Atmospheric anomalies are strongest in September–November because of a combination of a rather strong zonal SST gradient with the warmest SST in the equatorial Pacific just west of the dateline. The cold CP and EP events are associated with a southwestward shift of the South Pacific Convergence Zone with strongest atmospheric anomalies during the CP events. Squared wavelet coherence between NC rainfall and Niño 4 SST index shows that their negative correlations are mostly carried by two distinct timescales: the classical El Niño–Southern Oscillation (i.e., 3–6 years) variability and a quasi-decadal one (i.e., 10–12 years). The high-frequency (>1/8 cycle per year) correlations peak around Christmas and are quasi-stationary since 1950, whereas the low-frequency ones (<1/8 cycle per year) peak from the austral autumn to the austral spring and have strengthened from ~1975 to 1980 onward with a subtle warming trend in the equatorial Pacific near the dateline.

Citation: Barbero, R., and V. Moron (2011), Seasonal to decadal modulation of the impact of El Niño–Southern Oscillation on New Caledonia (SW Pacific) rainfall (1950–2010), *J. Geophys. Res.*, *116*, D23111, doi:10.1029/2011JD016577.

1. Introduction

[2] Rainfall anomalies across the South West (SW) tropical Pacific, including eastern Australia, are very sensitive to the spatial location and temporal phase of the South Pacific Convergence Zone (SPCZ) [*Vincent*, 1994; *Vincent et al.*, 2009]. This northwest–southeast (NW–SE) band of heavy rainfall tends to shift southwestward during La Niña (LN) and northeastward during El Niño (EN) events, when it usually merges with the equatorial Pacific Intertropical Convergence Zone (ITCZ) close to the dateline [*Vincent*, 1994]. New Caledonia (NC; ~166°E, 22°S) is located SW of the main axis of the climatological location of the SPCZ and is thus very sensitive to its anomalies in intensity and location. *Morlière and Rébert* [1986] showed that from 1950 to 1985, NC experienced a rainfall shortage (22% in mean) during an EN event from April to May of the following year. However, they showed that the correlation between the monthly Southern Oscillation Index (SOI) and the first empirical orthogonal function (EOF) of standardized NC rainfall was less than 0.3. *Nicet and Delcroix* [2000] found a higher correlation ($r = 0.54$) using low-pass filtered monthly values from 1969 to 1998, but the magnitude of NC rainfall anomalies is still not well hindcast by a linear regression using the SOI as the predictor. In fact, moderate EN events in 1992–1993 and 2002–2003 led to strong droughts in NC [*Fischer et al.*, 2004], while the major 1997–1998 EN event was not associated with large negative rainfall anomalies. *Wang and Hendon* [2007] also found that eastern Australia rainfall anomalies are more sensitive to the sea surface temperature (SST) anomalies (SSTAs) located on the eastern edge of the Pacific warm pool rather than those located in the eastern Pacific (EP), where SSTAs are the strongest. *Fischer et al.* [2004], using a nonlinear nonparametric spline regression, found that the highest negative rainfall anomalies in NC between 1951 and 2002 are associated with a standardized Niño 4 SST index close to 0.9 and with a standardized Niño 3 SST index near 0.62, resembling a warm EN event peaking near the dateline.

[1]Université d'Aix-Marseille, CEREGE, UMR 6635, Aix-en-Provence, France.
[2]Institut Universitaire de France, Paris, France.
[3]International Research Institute for Climate and Society, The Earth Institute, Columbia University, Palisades, New York, USA.

0148-0227/11/2011JD016577

[3] In fact, numerous studies have diagnosed recent changes in the spatiotemporal evolution of the EN events [e.g., *Guilderson and Schrag*, 1998]. Warm SSTA of most EN events that occurred before 1976 tended to spread westward from the EP, while the most recent EN events tend to spread eastward from the central Pacific (CP) [e.g., *Trenberth and Stepaniak*, 2001]. *Ashok et al.* [2007] defined the EN Modoki events as warm SSTAs in the CP, flanked by cold SSTAs on its eastern and western sides, leading to an anomalous ascendance throughout the whole troposphere close to the dateline. The possible disadvantage of this simple ad hoc definition is the correlation between the monthly El Niño Modoki Index (EMI) and the Niño 3 SST index ($r \sim 0.38$). This correlation leads to an unclear distinction between the Modoki and the EP events [*Feng et al.*, 2010a, 2010b]. *Kao and Yu* [2009] used a more objective and comprehensive approach to distinguish the EP from the Modoki or the CP events. The monthly SSTAs in the tropical Pacific (120°E–80°W, 20°S–20°N) are independently regressed onto Niño 1 + 2 and Niño 4 SST indices using a least squares regression. The leading principal component (PC) of the residuals from Niño 1 + 2 and Niño 4 SST indices defines the CP and EP events, respectively. Distinct teleconnections between the Modoki or CP events on one hand and the EP events on the other have been established in many areas including South America [*Hill et al.*, 2009], Australia and northern New Zealand [*Taschetto et al.*, 2009; *Taschetto and England*, 2009; *Wang and Hendon*, 2007], where the EN Modoki events induce stronger negative rainfall anomalies than the classical ones [*Weng et al.*, 2007].

[4] Over a longer timescale, *Folland et al.* [2002] showed that the SPCZ location is significantly linked with the Interdecadal Pacific Oscillation (IPO), a 15–30 year mode of variation of SSTA across the whole Pacific basin [*Power et al.*, 1999; *Chao et al.*, 2000]. The Pacific Decadal Oscillation (PDO) is usually seen as the northern component of the IPO [*Mantua et al.*, 1997]. The positive (negative) IPO phase displays a warm (cold) SSTA in the tropical Pacific, flanked by cold (warm) SSTA to the north and south. The negative phase of the IPO (e.g., from the mid-1940s to the mid-1970s and then from the late 1990s) is associated with a southwestward shift of the SPCZ, while the positive phase of the IPO from the late 1970s to the late 1990s is associated with a northeastward shift of its mean location [*Folland et al.*, 2002]. *Power et al.* [1999, 2006] also showed that the positive phase of the IPO decreases the interannual correlation between the El Niño–Southern Oscillation (ENSO) and Australia rainfall. Similarly, *Micevski et al.* [2005] showed that the relationship between the ENSO and eastern Australia rainfall anomalies is far stronger during the negative IPO phase.

[5] Here we analyzed the intra-annual to multidecadal variability of ENSO-related rainfall anomalies in NC based on a robust network of 22 stations from 1950 to 2010. This study has been triggered by recent changes in the ENSO evolution and its impacts over Australia [e.g., *Taschetto et al.*, 2009]. Moreover, the location of NC provides a good proxy of ENSO variations and enables an analysis of ENSO impacts in a different context than in Australia. Several SST indices, which include Niño's boxes, EMI, CP and EP indices, were compared. Then we focused on the atmospheric response associated with the EP and CP EN and LN events throughout the SW tropical Pacific. Finally, we investigated the multiscale modulation of the relationship between the ENSO and NC rainfall anomalies using the wavelet analysis.

2. Data

[6] Twenty-two rain gauge stations in NC with less than 10% of missing entries were used from 1950 to 2010 (Figure 1). Three stations were set up in 1950, whereas all 22 stations were operational from 1953. The rain gauges are located rather homogeneously along the leeward (i.e., west) and windward (i.e., east) coasts (Figure 1). The annual peak of rainfall occurs between December and April (up to 8 mm/d), when the SPCZ reaches its southernmost latitude. The leeward coast is always drier than the windward one (Figure 1). This opposition is attributed to the orographic forcing of the dominant easterly Alizean flow by the central range of mountains [*Lefèvre et al.*, 2010]. Local-scale rainfall from the NC network have been summed up over sliding 3 month periods and then standardized to zero mean and unit variance based on the available period to enhance the signal-to-noise ratio. Rainfall anomalies in the SW Pacific (110°E–260°E, 20°N–40°S) were computed in the same way using the monthly Climate Prediction Center's Merged Analysis of Precipitation (CMAP) from 1979 to 2010 [*Xie and Arkin*, 1996]. In this case, only post-1979 events were included in the composites analysis. Tropospheric wind anomalies were obtained from the first reanalyses of National Centers for Environmental Prediction (NCEP) [*Kalnay et al.*, 1996] and from the 20th-century reanalyses [*Compo et al.*, 2011] on the 1950–2010 period. The CMAP and NCEP data were processed in the same way as NC rainfall.

[7] Five monthly ENSO indices have been extracted from Extended Reconstructed SST (ERSST) data set (version 3b) from January 1950 to December 2010 [*Smith et al.*, 2008]: Niño 1 + 2, that is, averaged SSTAs over the box (90°W–80°W, 10°S–0°S), Niño 3 (90°W–150°W, 5°S–5°N), Niño 4 (160°E–150°W, 5°S–5°N), Niño 3.4 (120°W–170°W, 5°S–5°N), and EMI defined by *Ashok et al.* [2007] as EMI = [SSTA]c − 0.5[SSTA]e − 0.5[SSTA]w where the brackets represent the spatially averaged SSTAs in areas C (165°E–140°W, 10°S–10°N), E (110°W–70°W, 15°S–5°N), and W (125°E–145°E, 10°S–20°N). The CP and EP indices are computed as in the study by *Kao and Yu* [2009]. All the SST indices are averaged on a sliding 3 month period to fit with NC rainfall time series.

[8] To analyze the long-term relationships between Pacific SST and NC rainfall, the IPO and PDO indices were computed from January 1950 to December 2010. The PDO index is defined as the first EOF of Pacific SSTAs north of 20°N [*Mantua et al.*, 1997], while the IPO index is defined as the first EOF of detrended and low-pass filtered Pacific SSTAs [*Power et al.*, 1999; *Folland et al.*, 2002]. Previous authors used a cutoff of 13 years [*Mantua et al.*, 1997; *Power et al.*, 1999; *Folland et al.*, 2002]. Here we used a shorter cutoff of 8 years, as a longer period greater than 10–12 years potentially mixes two distinct bands of the teleconnection between ENSO and NC (see section 3.3). In both cases, the PCs were computed from standardized (zero mean and unit variance) monthly SSTAs extracted from ERSST version 3 and weighted by the squared cosine of the latitudes. This weights

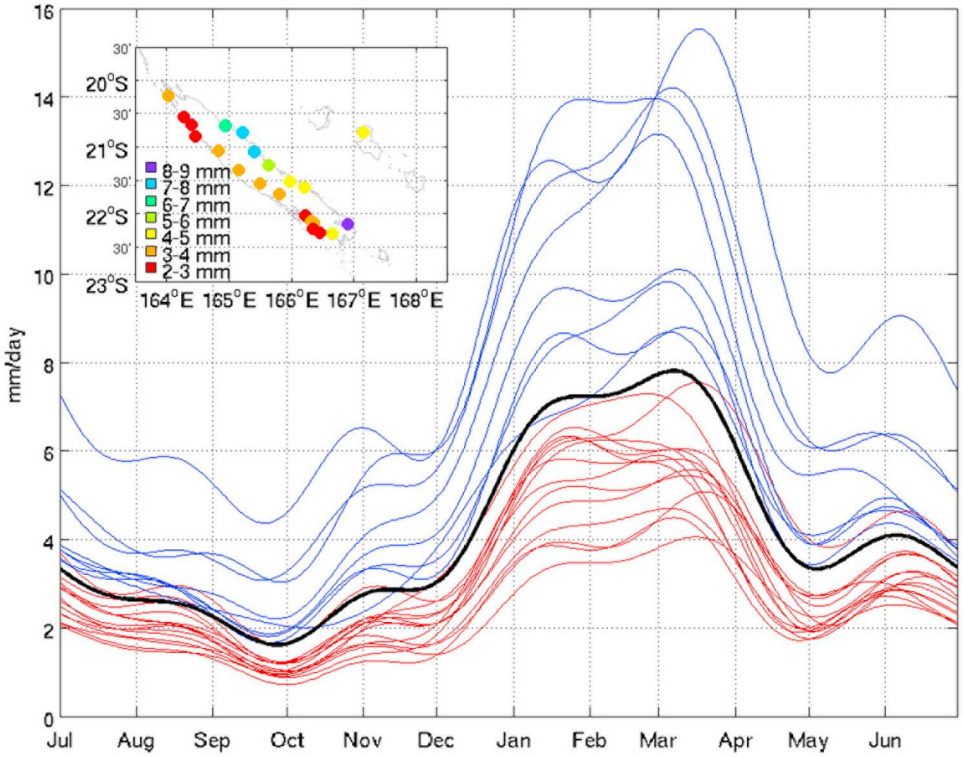

Figure 1. Mean annual rainfall (mm/d) of the 22 stations (red lines for the leeward coast, blue lines for the windward coast, and black line for the spatial average) during the period 1950–2010. The mean of each station is first computed as daily average and then low-pass filtered with a recursive Butterworth filter with a cutoff at 1/60 cycle per day. The insert in the top left corner is the mean daily rainfall for the 22 stations.

the variance of each grid point according to their latitude in the covariance matrix. The monthly time series of the PCs are then averaged over running 3 month periods to be consistent with the other indices used in this article.

3. Results

3.1. Spatial Scale of Seasonal Rainfall Anomalies Across NC and in the SW Pacific

[9] The Standardized Anomaly Index (SAI) of NC is computed as the spatial average of 22 local-scale standardized anomalies, without any missing entries being filled in [*Katz and Glantz*, 1986; *Moron et al.*, 2007]. The interannual variance of the SAI (Var(SAI)) is a measure of the in-phase spatially coherent variability across NC and ranges from 0.73 in February–April (FMA) to 0.82 in September–November (SON) with a mean value of 0.78 across the 12 trimesters. Note that Var(SAI) may be 1 if all stations are perfectly positively correlated, 0.0455 (= 1/22) in the case of any independent variations among the 22 stations, and 0 if 11 stations are perfectly out of phase with the remaining ones [*Katz and Glantz*, 1986]. So, Var(SAI) indicates here a large in-phase interannual variability of seasonal rainfall anomalies across NC. Hereafter, the SAI of NC rainfall is simply referred to as NC rainfall. Figure 2 shows the seasonal mean rainfall in the SW Pacific and its correlations with NC rainfall during the four seasons in the 1979–2010 period. The highest positive correlations do not necessarily peak over NC, suggesting that CMAP do not include NC rain gauges. The scale of NC-related rainfall anomalies is largest in December–February (DJF) (Figure 2c) and especially in SON (Figure 2b), and smallest in June–August (JJA) (Figure 2a). Positive and negative correlations usually stretch SW, including NC, and NE of the climatological axis of the SPCZ. This suggests that NC reflects, at least in part, the SW–NE shift of the SPCZ and its possible merging with ITCZ in the central equatorial Pacific. This pattern is well established in SON (Figure 2b) and then weakens to almost disappear in JJA (Figure 2a). Note that the largest scale in SON corresponds to the largest intra-NC spatial coherence (i.e., maximum of Var(SAI)).

3.2. Seasonal Modulation of ENSO Impacts Over NC Rainfall

[10] Correlations between ENSO indices and NC rainfall peak from August–October (ASO) to January–March (JFM) with a maximum around October–November (Figure 3). The strongest correlations are found with CP SSTA indices (i.e., Niño 4 and CP), while EP index is not significantly correlated with NC rainfall. Correlations with all ENSO indices are weaker during the austral winter (Figure 3), because NC rainfall is then partly caused by extratropical perturbations and tropical/extratropical interactions that are not necessarily related to ENSO. Moreover, ENSO teleconnections are still relatively weak during the austral winter. The following composite analyses start from the SON season, which roughly coincides with (1) the middle and end part of the dry season (Figure 1), (2) the usual developing phase of ENSO events,

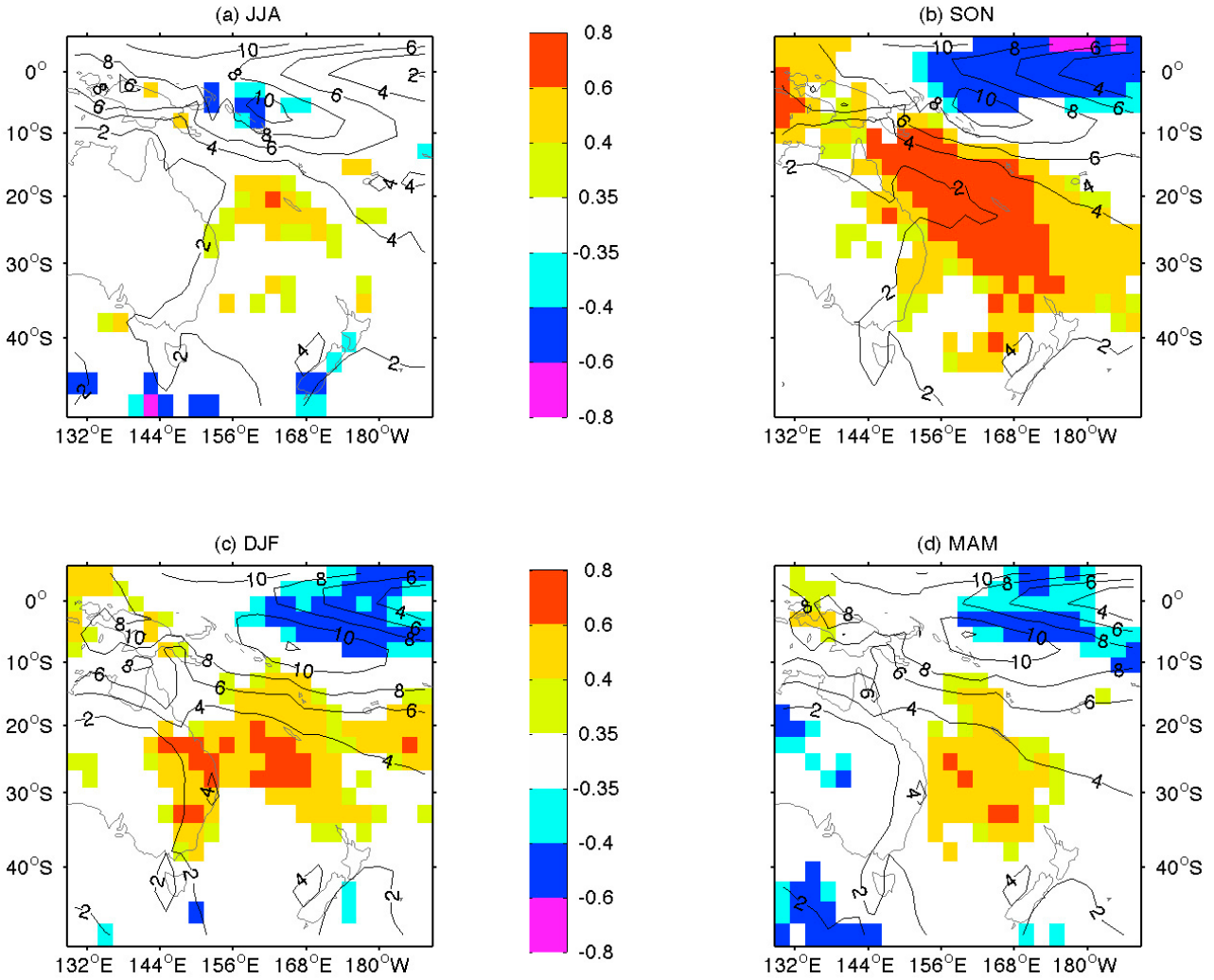

Figure 2. Mean Climate Prediction Center's Merged Analysis of Precipitation rainfall (mm/d) in (a) June–August (JJA), (b) September–October (SON), (c) December–February (DJF), and (d) March–May (MAM) computed on running 3 month periods (gray contours) and correlations (shaded colors) between standardized CMAP anomalies and Standardized Anomaly Index (spatial average of local-scale anomalies) of NC rainfall during the period 1979–2010. Only significant correlations at the two-sided 95% level according to the random phase test [*Janicot et al.*, 1996] are plotted.

and (3) the largest spatial scale of NC-related rainfall anomalies (Figure 2b).

3.3. Different Patterns of EN Impacts in NC and Throughout the SW Pacific

[11] NC rainfall anomalies in SON are composited using the 15%, 20%, 25%, 30%, and 33% lower percentiles (e.g., cold events) and upper percentiles (e.g., warm events) of ENSO events from EMI, Niño 4, EP, CP, and Niño 3 SST indices (Tables 1 and 2). The values in Tables 1 and 2 indicate the mean NC rainfall anomalies associated with the EN events, which occur above the upper percentiles and LN events, which occur below the lower percentiles, respectively. We used various percentiles to avoid ad hoc samples and misinterpretation of our composites. The NC rainfall anomalies (Tables 1 and 2) are in agreement with the preceding negative correlations (Figure 3). Note that the magnitude of rainfall anomalies does not necessarily increase with the magnitude of warm and cold EN events except with Niño 4 SST index. These results indicate that the warm EP events are systematically uncorrelated with NC rainfall, while the warm CP or Niño 4 events always result in a significant drought (Table 1). Negative rainfall anomalies associated with the 25%–33% warmest EN events based on EMI and Niño 3 index are significant at the two-sided 95% level, but the ones related to the 20% warmest EN Modoki events do not reach this level of significance. This result suggests that ENSO impact is better detected in NC with CP indices (CP or Niño 4), whereas using EMI and Niño 3 index to distinguish the impact from different types of ENSO is more ambiguous.

[12] The standardized regional-scale rainfall and 850 hPa NCEP wind anomalies in the SW Pacific associated with the 15% upper percentiles (e.g., warmest) CP (1963, 1965, 1977, 1986, 1987, 1990, 1991, 1994, and 2009) and EP (1951, 1965, 1972, 1976, 1982, 1983, 1997, 1998, and 2008) events

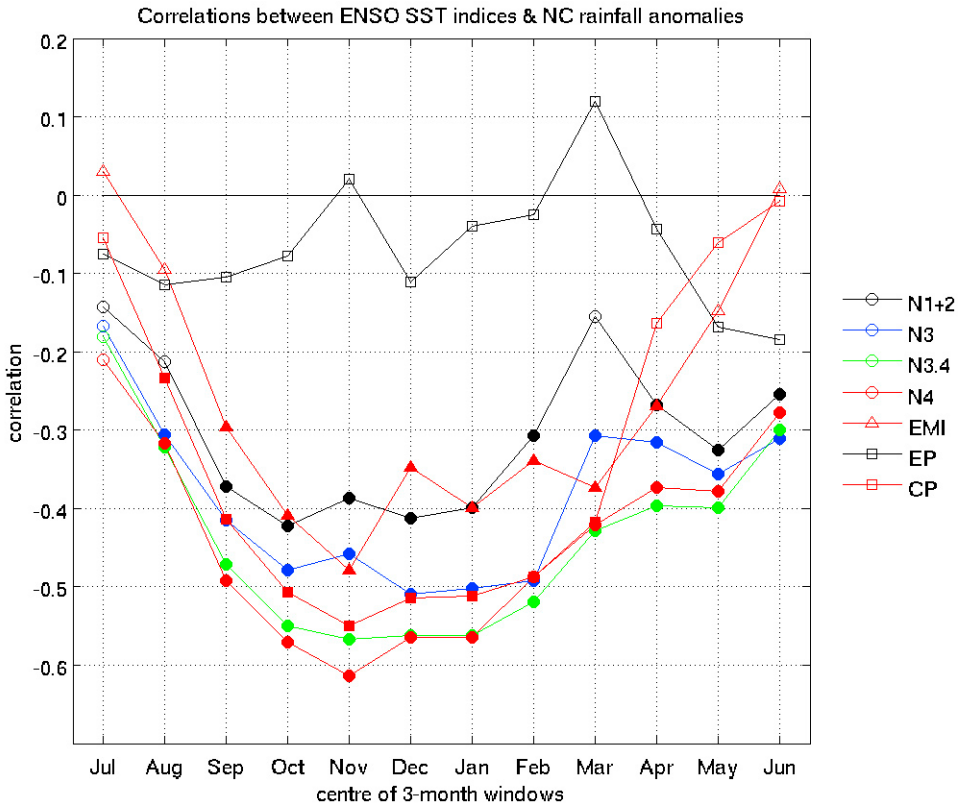

Figure 3. Correlations on running 3 month periods between Standardized Anomaly Index of NC rainfall and various ENSO SST indices (Niño 1 + 2, Niño 3, Niño 3.4, Niño 4, CP, EP, and EMI) for the 1950–2010 period. Filled symbols indicate significant correlations at the two-sided 95% level according to the random phase test [*Janicot et al.*, 1996]. The ENSO indices are described in section 2.

in SON are averaged in Figures 4a and 4b. Note that the years 1963, 1983, and 1991 were under the impact of the biggest volcanic eruptions of the 20th century but do not affect the results presented in the following. Significant eastward wind anomalies at 850 hPa along the equator are associated with the characteristic horseshoe structure of rainfall anomalies during the EP events (Figure 4a). Positive rainfall anomalies peak in the equatorial east Pacific, and negative anomalies reach their highest amplitude in the tropical central Pacific south of 20°S east of the dateline, and the whole tropical Pacific north of 5°N. The NC is located southwest of the NW–SE band of significant negative rainfall anomalies. During the CP events (Figure 4b), rainfall anomalies are almost in quadrature with the ones associated with the warm EP events. In particular, the positive rainfall anomaly shifts toward the equatorial west Pacific between 155°E and 170°W, and significant negative anomalies now cover the whole SW Pacific between NC and the northeastern coast of Australia (Figure 4b). Similarly, local-scale rainfall anomalies in SON are near normal during EP events (including the two strongest events of the century in 1982 and 1997) and significantly negative at the 22 Météo-France stations during CP events (not shown).

Table 1. September–November Standardized Anomalies Index of NC Rainfall Computed From Niño 3, El Niño Modoki Index, Eastern Pacific, Central Pacific, and Niño 4 SST Indices Using the Upper 15%, 20%, 25%, 30%, and 33% Percentiles (e.g., Warm Events)[a]

Percent	Niño 3	EMI	EP	CP	Niño 4
33	−0.52*	−0.40*	0.15	−0.53*	−0.49*
30	−0.51*	−0.37*	0.18	−0.60*	−0.56*
25	−0.48*	−0.34*	−0.09	−0.61*	−0.57*
20	−0.39*	−0.36	−0.03	−0.50*	−0.66*
15	−0.31	−0.39*	0.12	−0.47*	−0.68*

[a]Asterisks indicate significant anomalies at the two-sided 95% level according to a Student's *t* test compared to the 1950–2010 climatology. September–November, SON; Standardized Anomalies Index, SAI; El Niño Modoki Index, EMI; Eastern Pacific, EP; Central Pacific, CP.

Table 2. September–November Standardized Anomalies Index of NC Rainfall Computed From Niño 3, El Niño Modoki Index, Eastern Pacific, Central Pacific, and Niño 4 SST Indices Using the Lower 15%, 20%, 25%, 30%, and 33% Percentiles (e.g., Cold Events)[a]

Percent	Niño 3	EMI	EP	CP	Niño 4
33	0.72*	0.59*	0.18	0.68*	0.53*
30	0.66*	0.67*	0.26	0.78*	0.63*
25	0.56*	0.81*	0.27	0.75*	0.70*
20	0.69*	0.62*	0.51	0.76*	0.75*
15	0.70*	0.49*	0.43*	0.54*	0.76*

[a]Asterisks indicate significant anomalies at the two-sided 95% level according to a Student's *t* test compared to the 1950–2010 climatology. September–November, SON; Standardized Anomalies Index, SAI; El Niño Modoki Index, EMI; Eastern Pacific, EP; Central Pacific, CP.

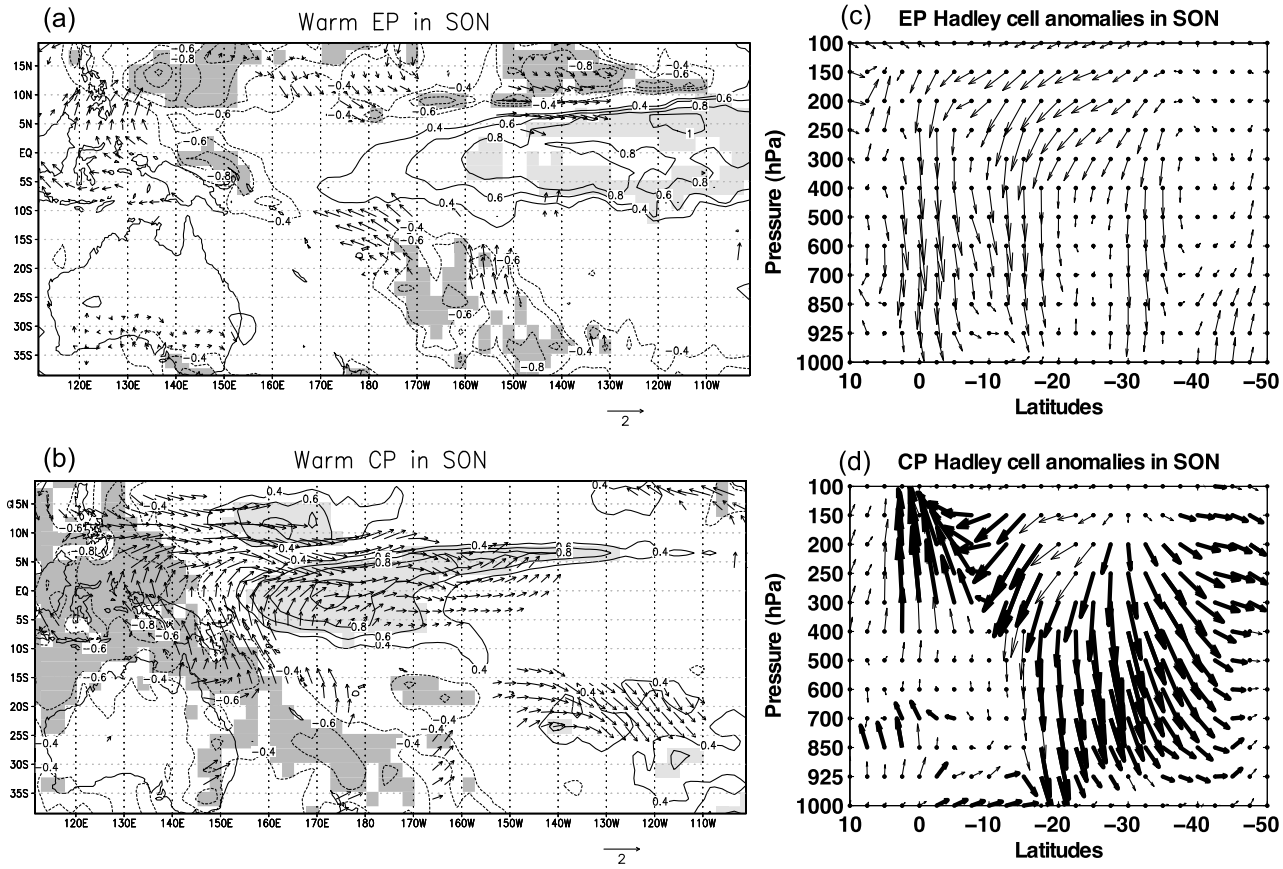

Figure 4. Composites of standardized rainfall and 850 hPa wind anomalies in SON relative to the 1950–2010 long-term mean over the SW Pacific during the upper 15% percentiles of (a) EP events (i.e., 1951, 1965, 1972, 1976, 1982, 1983, 1997, 1998, and 2008) and (b) CP events (i.e., 1963, 1965, 1977, 1986, 1987, 1990, 1991, 1994, and 2009) during the period 1950–2010 for the winds and during the period 1979–2010 for the rainfall. Dark (light) gray shading indicates significant negative (positive) rainfall anomalies versus long-term mean at the two-sided 95% level according to a Student's *t* test. Anomalous Hadley circulation relative to the 1950–2010 long-term mean during the upper 15% percentiles of (c) EP and (d) CP events in SON (1950–2010) is represented by vectors consisting of the meridional wind anomaly (horizontal component; units: m s^{-1}) and pressure vertical velocity anomaly (vertical component scaled by -2×10^{-2} Pa s^{-1}) averaged over 160°E–170°E. Maximum vector magnitude is equal to 2.83 m s^{-1}. Vectors whose zonal or meridional components are significant at the two-sided 95% level are drawn in bold black.

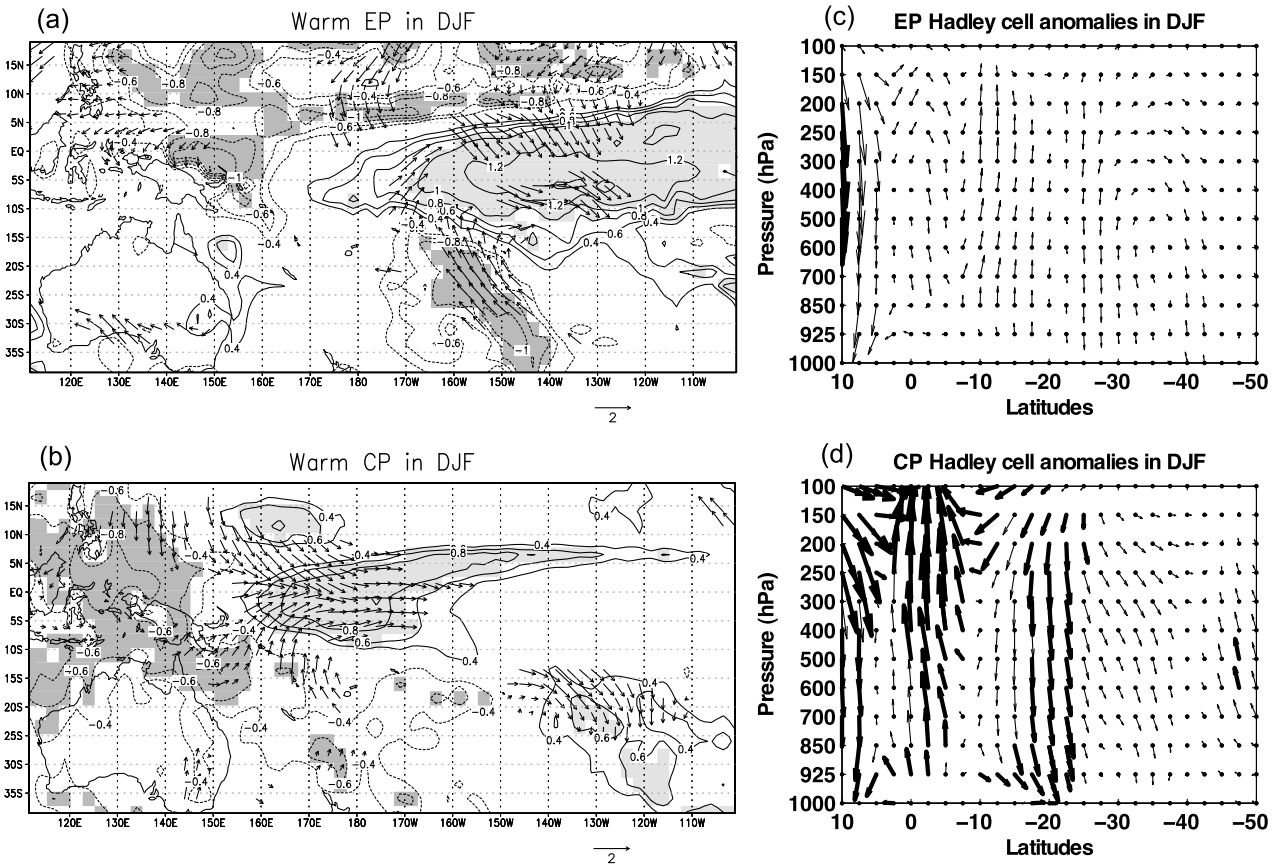

Figure 5. As in Figure 4 except for DJF.

[13] The Hadley circulation at NC longitudes is clearly modified during warm CP events (Figure 4d) compared to warm EP events (Figure 4c) with a clear anomalous upward branch near the equator, peaking in the upper troposphere in relation to the latent heat release associated with positive rainfall anomalies near the dateline. The anomalous descending branch in the austral hemisphere is weak and confined between the equator and 10°S during warm EP events (Figure 4c), while it is stronger and stretched to ~35°S, including NC, during warm CP events (Figure 4d). The results are very similar (not shown) when composites are computed from the 20th-century reanalysis data set [*Compo et al.*, 2011].

[14] The rainfall and wind composites are computed for the same set of years on the 12 sliding 3 month seasons from JJA to March–May (MAM) +1 after warm events. The DJF composites are shown in Figure 5. The SON atmospheric pattern (Figures 4a and 4b) emerges from around June–September (JAS; not shown) and persists in DJF during warm EP events (Figures 5a and 5b). During warm CP events (Figure 5b), the strong positive rainfall anomalies close to the equator are still associated in DJF with an anomalous upward motion in the whole troposphere (Figure 5d), while the negative rainfall anomalies over SW Pacific, including NC are now weaker than in SON and shift slightly northwestward. This typical atmospheric pattern tends to disappear in MAM (not shown) of the following year of the warm EP and CP events.

[15] The composites are also computed for the 15% lower (e.g., cold events) CP events (i.e., 1955, 1964, 1971, 1973, 1975, 1983, 1988, 1998, and 1999) and EP events (i.e., 1955, 1956, 1966, 1967, 1990, 1996, 2001, 2005, and 2007) in SON (Figure 6) and DJF (Figure 7). Note that while only one event (1955) belongs to both CP and EP samples, the atmospheric anomalies are pretty similar between the cold EP and CP events, either in SON (Figure 6) or in DJF (Figure 7), but the magnitude of the anomalies is larger during the cold CP events. Figure 6 displays a weak but not significant upward motion over NC during the cold EP (Figure 6c) events with weak positive rainfall anomalies SE of NC (Figure 6a) in SON. The cold CP events (Figure 6b) exhibit strong negative rainfall anomalies over the central Pacific and strong positive rainfall anomalies from Indonesia to SW Pacific, including NC. This pattern is associated with faster equatorial easterlies than usual and strong north to NW anomalies over the SW Pacific consistent with an anomalous advection of moisture and a southward shift of the SPCZ. Wind anomalies at 850 hPa (Figure 6b) are roughly reversed compared to the warm CP events (Figure 4b) and an anomalous upward branch is located over NC latitudes (Figure 6d). This pattern persists in DJF with negative rainfall anomalies that stretch southeastward in the SW Pacific during the cold CP events (Figure 7b). The atmospheric anomalies associated with the cold EP events are weaker (Figures 7a and 7c), as already observed in SON. Furthermore, this result suggests that atmospheric anomalies observed during a CP event are

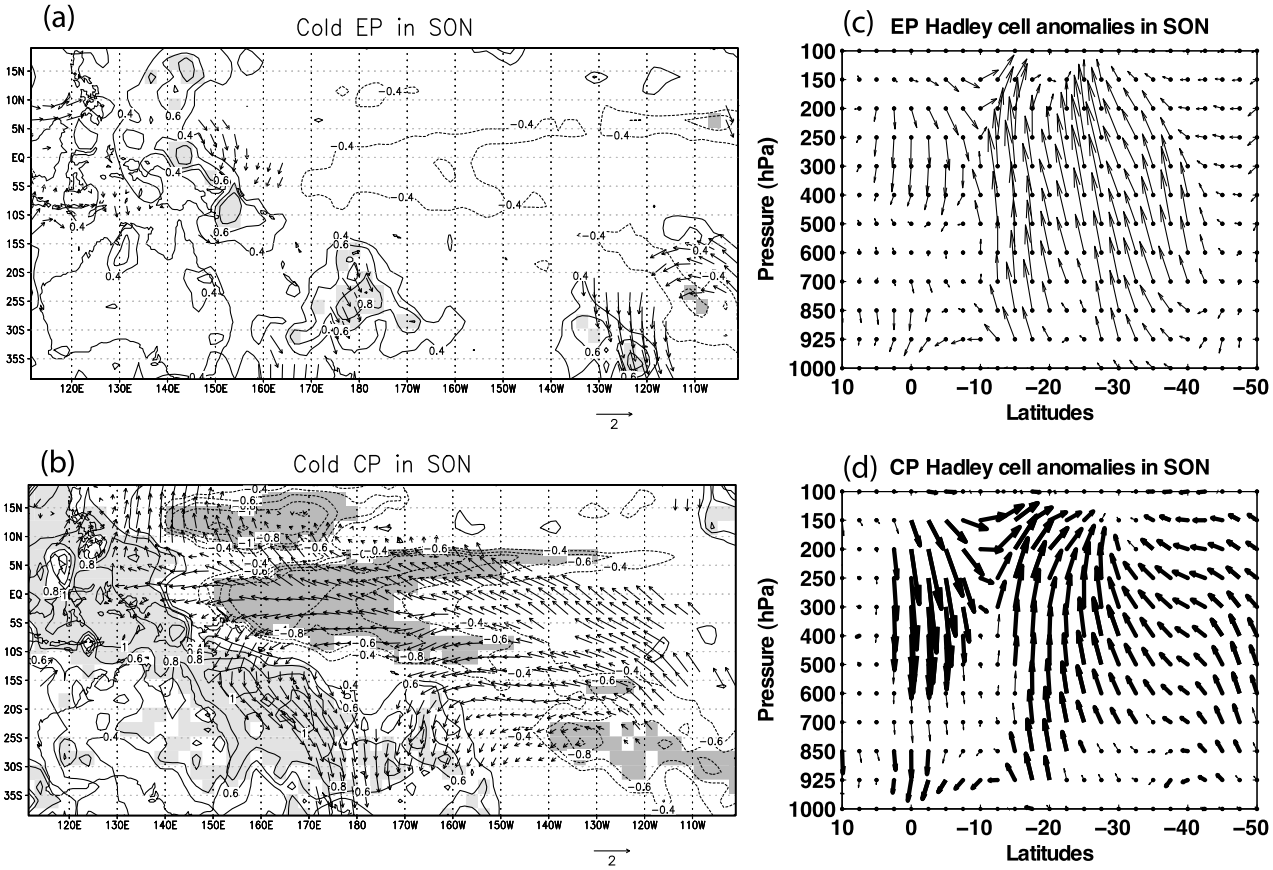

Figure 6. As in Figure 4 except for the lower 15% percentiles of EP events (i.e., 1955, 1956, 1966, 1967, 1990, 1996, 2001, 2005, and 2007) and CP events (i.e., 1955, 1964, 1971, 1973, 1975, 1983, 1988, 1998, and 1999).

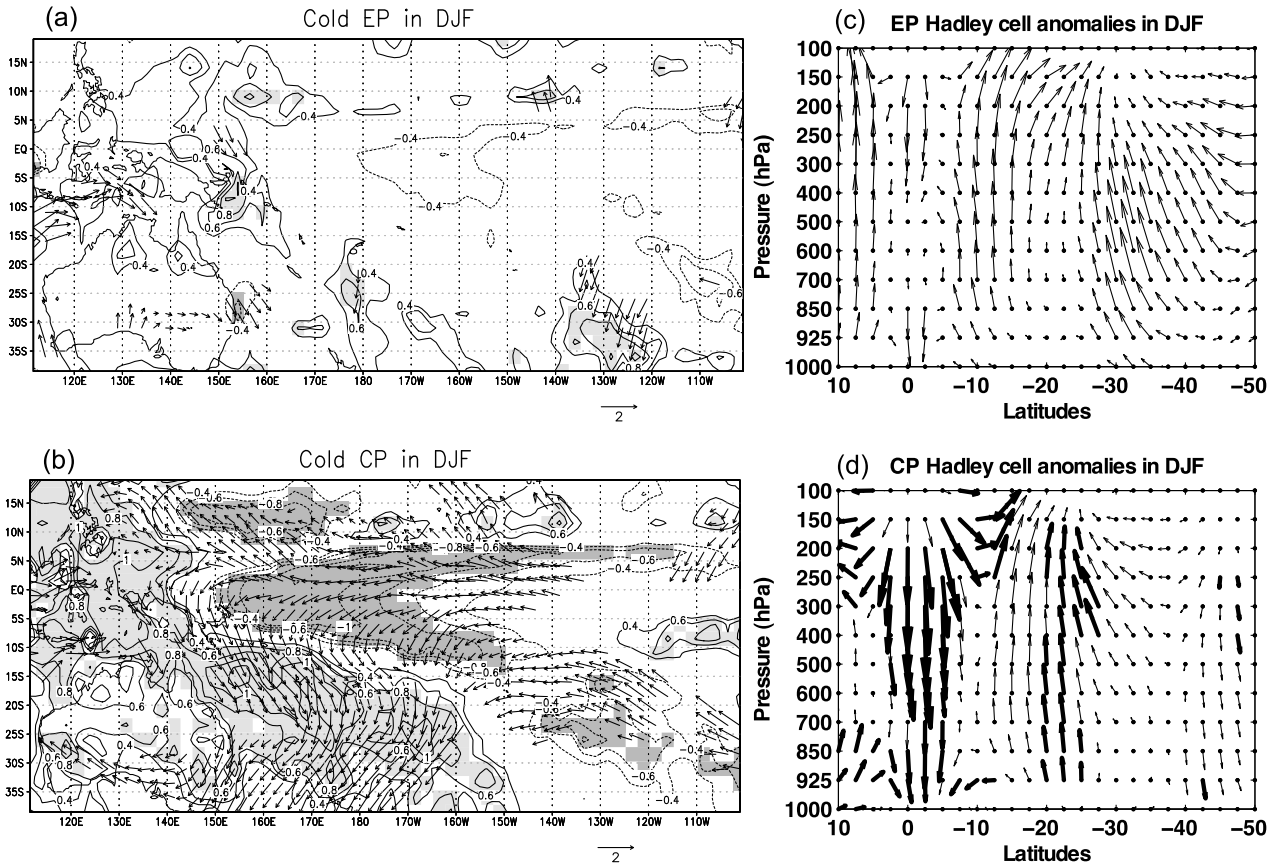

Figure 7. As in Figure 6 except for DJF.

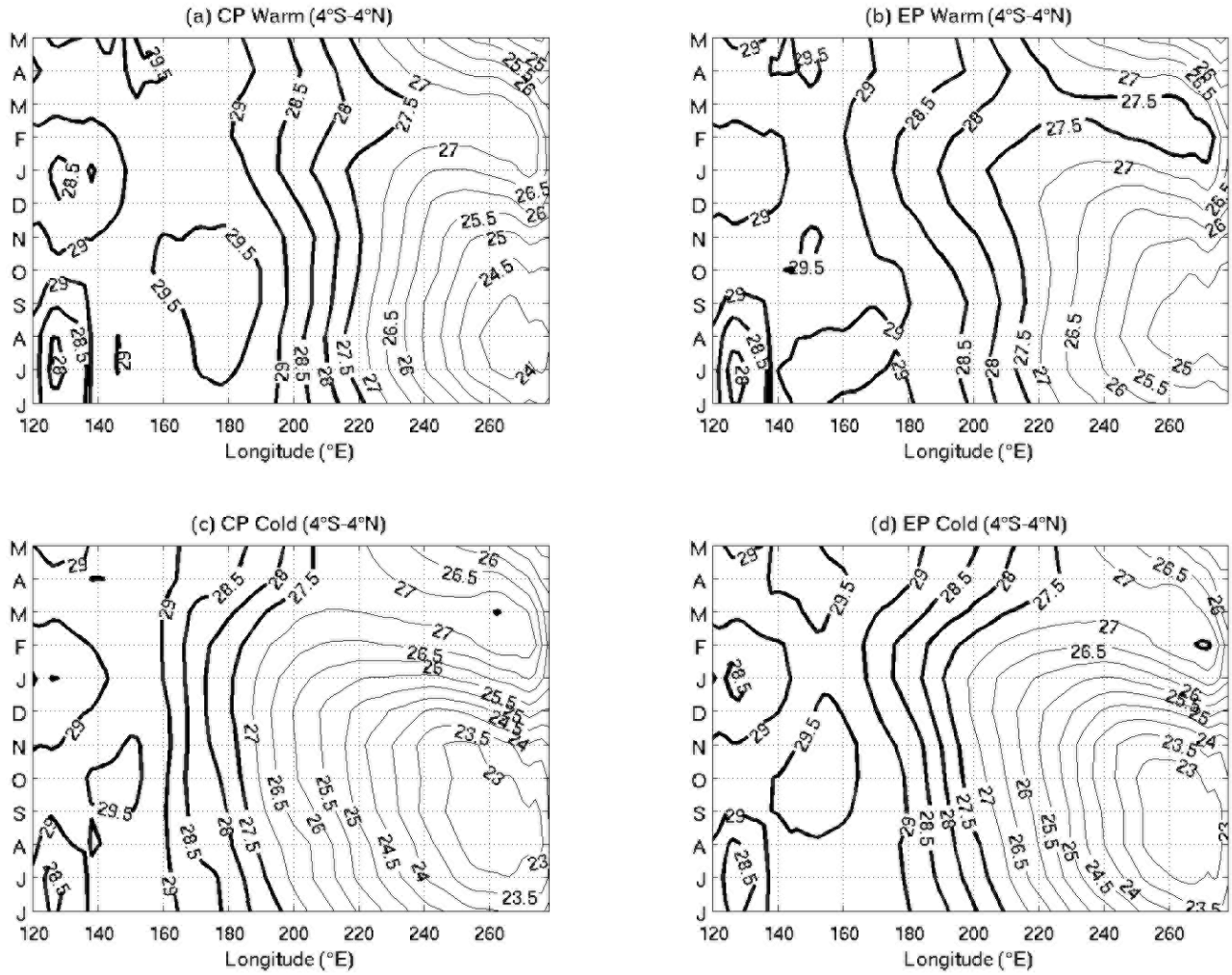

Figure 8. Time-longitude evolution of the SST averaged between 4°S and 4°N for the upper 15% percentiles of the (a) CP and (b) EP events and for the lower 15% percentiles of the (c) CP and (d) EP events defined from the SON season, from June to May of the following year.

roughly reversed between a warm and a cold event, while the amplitude of the anomalies is larger over the western Pacific during the latter event. In contrast, the warm EP events display larger anomalies than the cold EP ones.

[16] The fact that we found a relative similarity between cold CP and EP events composites and a large difference between warm CP and EP events could be related to the seasonal evolution of the CP and EP events themselves. Figure 8 shows the time-longitude variation of Pacific SST averaged between 4°N and 4°S for the upper 15% and lower 15% EP and CP events defined from the SON season, from June to May +1. The warm CP events (Figure 8a) exhibit a strong zonal dipole in SON with SST above 29.5 °C near the dateline, enhancing the deep equatorial convection there and thus reinforcing the associated descending meridional branch over NC latitudes. This zonal dipole largely weakens in JFM of the following year. This is mostly due to the superposition of the SSTAs to the annual flattening of the zonal SST gradient near and after Christmas. The zonal gradient is far weaker during warm EP events (Figure 8b) because of the strong warm SSTAs in the east. During cold events (Figures 8c and 8d), the zonal SST gradient is stronger than during warm CP events (Figure 8a) without strong differences between CP and EP events. Figure 9 highlights the strong seasonal zonal gradient along the equatorial Pacific during the warm CP events compared to the warm EP events. The deviation between warm CP and warm EP is strong around September and weakens after December, whereas there is no difference between the cold EP and cold CP events.

3.4. Temporal Modulation of the ENSO-NC Rainfall Relationships

[17] In section 3.3, we showed that NC rainfall variability is strongly modulated by SSTAs near the dateline approximately from September to March. In this section, we will investigate the possible temporal modulation of this relationship throughout the year through the wavelet analysis [*Grinsted et al.*, 2004]. Figure 10a shows the wavelet power spectra of the monthly Niño 4 SST index. Throughout the period, energetic oscillations stand out in the 3–6 year band. The wavelet power spectra of monthly NC rainfall

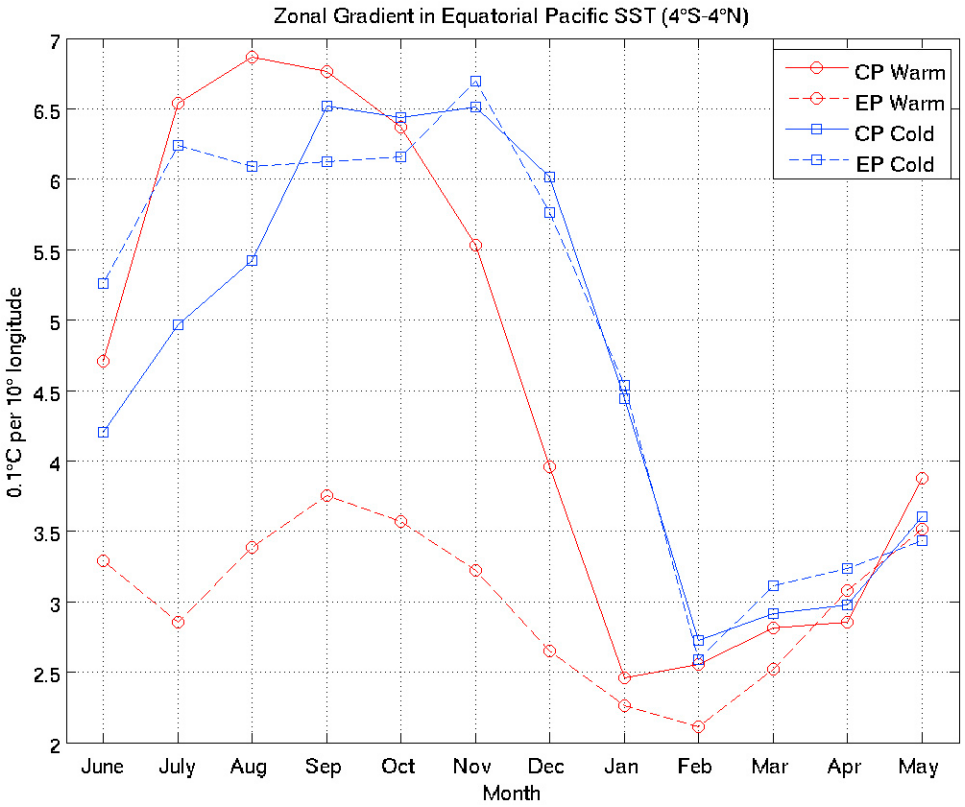

Figure 9. Zonal gradient (expressed in 1/10th of °C per 10° longitude) in the equatorial Pacific (in the 119°E–279°E box as in Figure 8) for the upper and lower 15% percentiles of CP and EP events. The zonal gradient is estimated as the difference between the maximum and minimum SSTs latitudinally averaged between 4°N and 4°S divided by their longitudinal distance. These composites are defined from the SON season, from June to May of the following year.

displays a noisy signal with some significant intermittent peaks in the 4–16 month band and 4–5 year band, especially around 1960 (Figure 10b) and at decadal timescale from the late 1970s. The squared wavelet coherence, which can be viewed as a localized correlation coefficient in time-frequency space [*Grinsted et al.*, 2004], shows that negative correlations between Niño 4 SST index and NC rainfall (Figure 3) are mostly carried by an antiphase relationship in the 3–6 year classical ENSO band and in the 10–12 year band (Figure 10c). The same results are obtained with the CP index (not shown).

[18] Thus, we return to the results of Figure 3 by considering separately the 3–6 year and the 10–12 year bands. The NC rainfall and Niño 4 SST time series (running 3 months) are low-pass filtered with a recursive Butterworth filter with a cutoff at 1/8 cycle per year. The high-pass residuals of this filter include the 3–6 year band. Correlations are computed on a 21 year running window on both frequencies and are displayed in the time-frequency domain [*Gaucherel*, 2009]. The high-pass correlations are at a maximum from SON to JFM, that is, near the largest annual amplitude of ENSO events (Figure 11a). These correlations are stationary throughout the whole period (Figure 11a). In contrast, the low-pass correlations (Figure 11b) are stronger from April–June (AMJ) to October–December (OND) and seem to have strengthened in recent decades.

[19] To understand better the interactions between NC rainfall and tropical Pacific SST in the low frequency, we compared NC rainfall variability with low-pass filtered (<1/8 cycle per year) PDO, IPO, and Niño 4 SST indices. Figures 12a and 12b display, respectively, the first EOF of monthly Pacific SSTAs north of 20°N (PDO) and the first EOF of detrended and low-pass filtered (<1/8 cycle per year) monthly Pacific SSTAs (IPO). Both EOFs are highly similar over the area they overlap, and the largest IPO weights are located away from the equator, even if IPO includes the classical horseshoe pattern associated with ENSO (Figures 12a and 12b) [*Zhang et al.*, 1997]. The IPO, low-pass PDO, and Niño 4 SST time series are highly correlated, while Niño 4 index exhibits a weak warming trend as from 1990, that is, neither present in IPO by definition nor in PDO (Figure 12c). These indices are negatively correlated with NC rainfall mostly from the 1970s onward (Figure 12c), suggesting that IPO/PDO could be involved in the recent increase of the ENSO-NC rainfall association in low frequency.

[20] Then we regressed tropical Pacific SSTAs onto NC rainfall for each season in high- and low-frequencies. Figure 13 shows SSTAs associated with negative rainfall anomalies = −1 standard deviation in NC. On one hand, the high-pass SSTA associated with negative rainfall anomalies in NC logically increases from JJA to SON (Figures 13a and 13c) and, on the other hand, decreases from DJF to

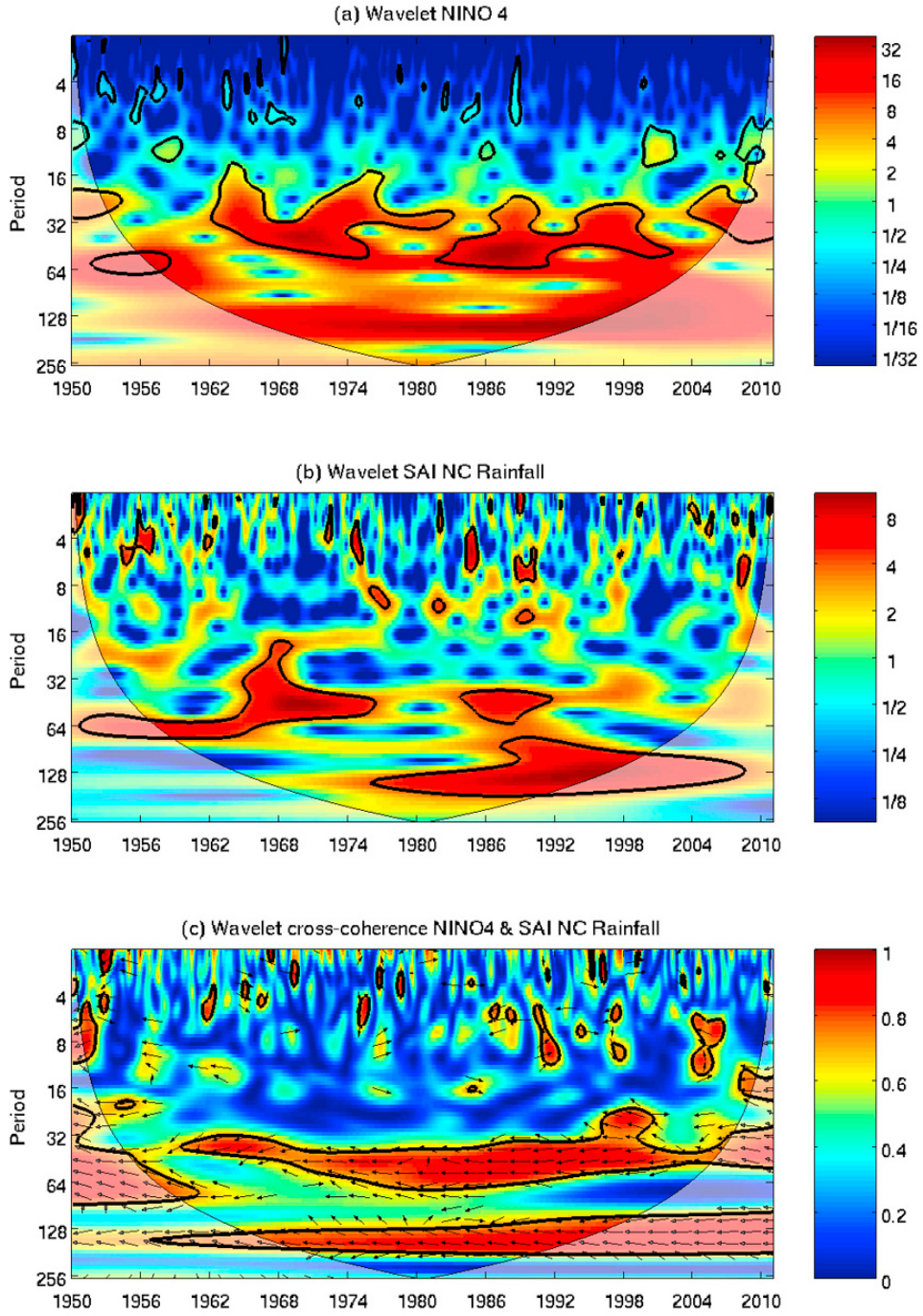

Figure 10. (a) Continuous wavelet power spectrum of the monthly Niño 4 SST index. (b) Continuous wavelet power spectrum of the monthly Standardized Anomaly Index (SAI) of NC rainfall. The SAI is computed as the spatial average of monthly rainfall anomalies over the 22 stations (Figure 1). (c) Squared wavelet coherence between the monthly SAI and Niño 4 SST index. The relative phase relationship is shown as arrows (with antiphase pointing left). The thick black contour designates the one-sided 95% significance level against red noise, and the cone of influence where edge effects might distort the picture is shown as a lighter shade [*Grinsted et al.*, 2004].

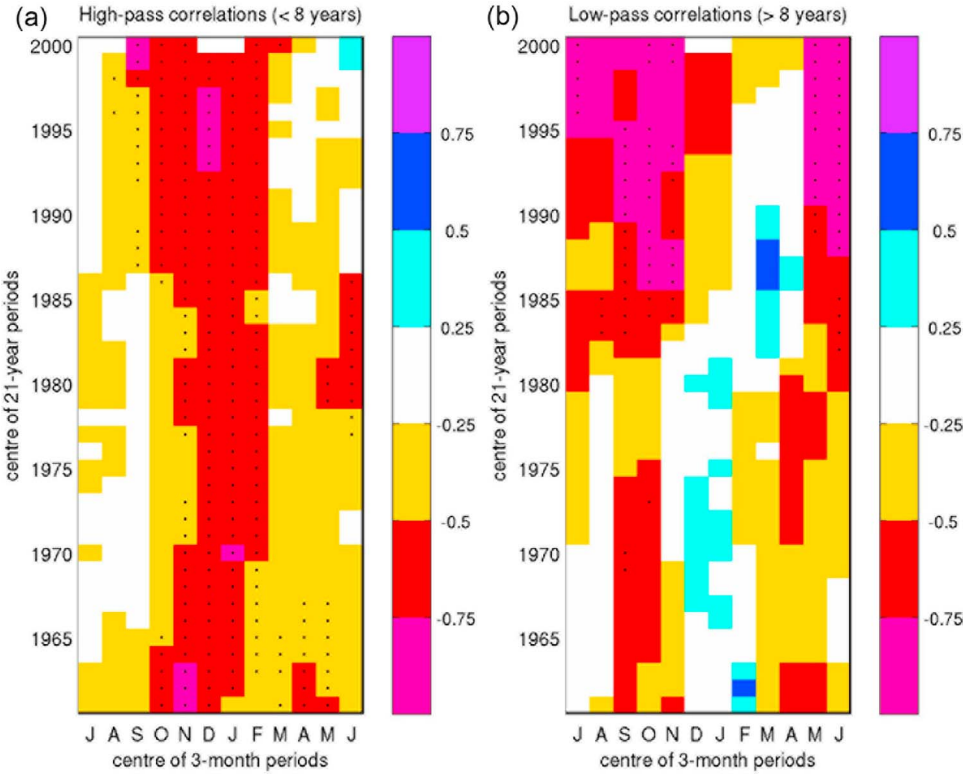

Figure 11. Correlations on running 21 year windows during the period 1950–2010 between the Standardized Anomaly Index (SAI) of 3 month local-scale rainfall anomalies in NC and Niño 4 SST index. (a) Both time series are the residuals of a low-pass recursive Butterworth filter with a cutoff at 1/8 cycle per year. (b) As in Figure 11a except low-pass filtered time series of SAI and Niño 4 are used. Black dots indicate significant local correlations at the two-sided 90% level according to a Monte Carlo random phase test [*Janicot et al.*, 1996].

MAM (Figures 13e and 13g). It is fully consistent with our previous results, that is, rainfall anomalies in NC are strongly related to ENSO phenomenon (Figure 3) and reflect larger teleconnections in SON/DJF than in MAM/JJA (Figure 2). The spatial structure of the high-pass SSTAs roughly matches the one usually associated with the ENSO events in SON and DJF and shows a very weak pattern in JJA (Figure 13a) and MAM (Figure 13g). In DJF, the largest SSTA related to NC droughts tend to shift eastward along the equator (Figure 13c), thus decreasing the influence of the CP events compared to SON. Over and above 8 years, positive SSTA peaks clearly in the CP in SON (Figure 13d) and then weakens in DJF (Figure 13f) and mostly in MAM (Figure 13h). It is consistent with the efficient superposition of slow and fast ENSO variations in SON. The SSTAs associated with positive rainfall anomalies equal to or more than a standard deviation of 1 in NC display the same seasonal patterns, except in SON in the low frequency, where the SSTA pattern is similar to PDO-IPO (not shown).

4. Discussion and Conclusion

[21] We analyzed the interannual variability of 3 month rainfall in NC (~22°S, 166°E) from a data set of 22 stations from 1950 to 2010. This study was motivated by previous works about the sensitivity of rainfall anomaly pattern (especially in Australia) to different types of ENSO events and by the location of the NC in a very sensitive region to SPCZ displacements. A simple spatial average of the local-scale standardized anomalies can be used to summarize interannual variability, thanks to the strong in-phase covariance among the 22 stations. The spatial scale of rainfall anomalies linearly related to NC is found to be the largest in SON and the smallest in JJA. The spatial pattern of correlations between CMAP and NC rainfall anomalies suggests that NC rainfall anomalies not only reflect in SON but also in DJF, a large-scale pattern, associated in part with the location of the SPCZ. This is fully consistent with the study by *Salinger et al.* [1995], who argued that SPCZ displacements can result in very large precipitation anomalies on either side of its mean location.

[22] The negative correlations between NC rainfall and ENSO phenomenon peak between ASO and JFM, when ENSO strengthens and usually reaches its highest annual amplitude. The weaker correlations are observed from the austral autumn to the austral spring when ENSO tends to switch from the warm to cold phases and vice versa and when NC rainfall could be impacted by extratropical-tropical interactions and middle-latitude processes [*Gillett et al.*, 2006], poorly related to the ENSO phenomenon. The correlations between NC rainfall and ENSO phenomenon are

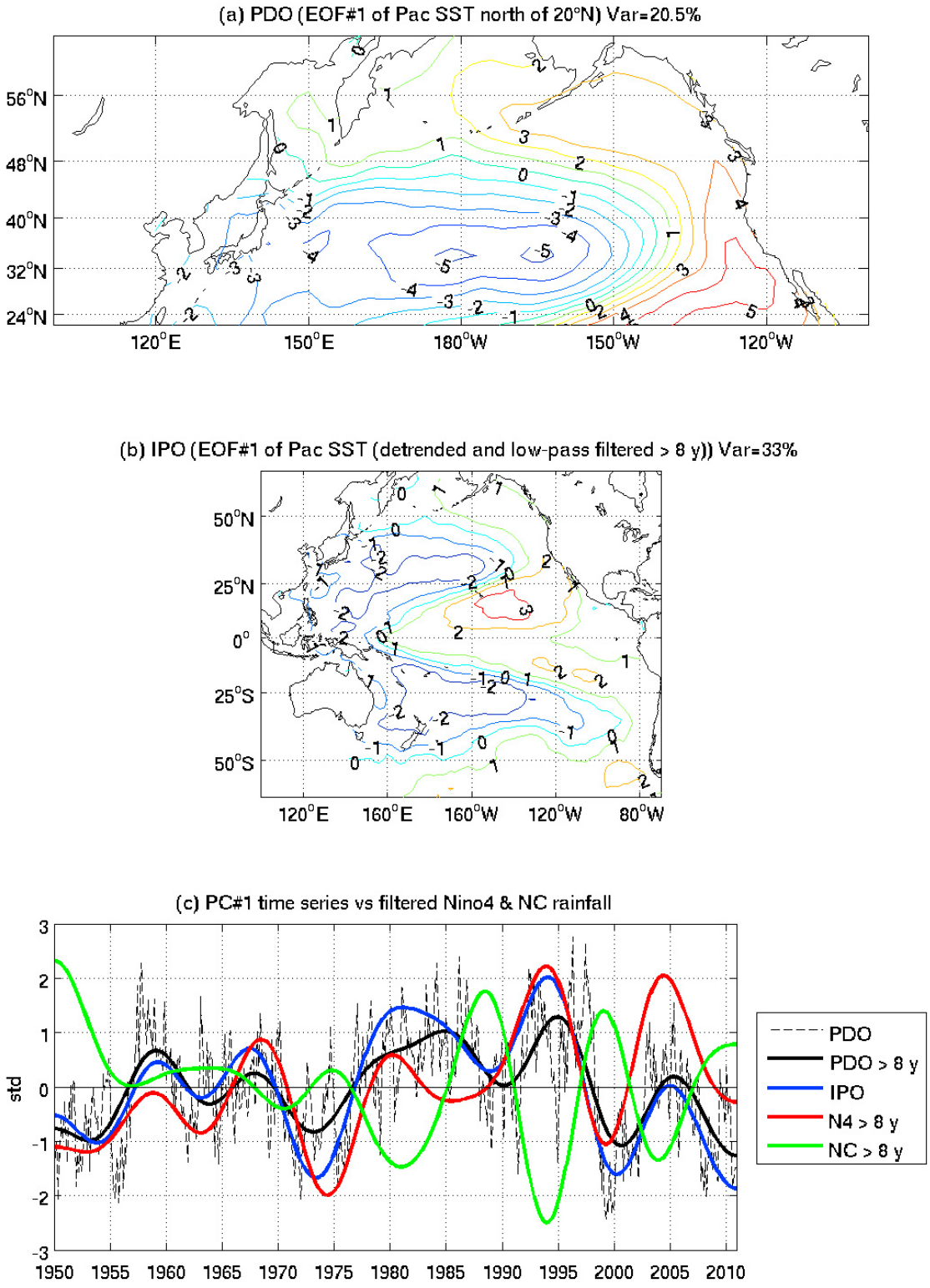

Figure 12. (a) The PDO pattern defined as the first empirical orthogonal function (EOF) of Pacific SSTAs north of 20°N (1950–2010). (b) The IPO pattern defined as the first EOF of Pacific SST detrended and low-pass filtered (>8 years) during the same period. (c) Temporal score time series of the PDO low-pass filtered (bold black line) and unfiltered (dashed black line), the IPO (bold blue line), the Niño 4 SST index low-pass filtered (>8 years), and NC rainfall low-pass filtered (>8 years).

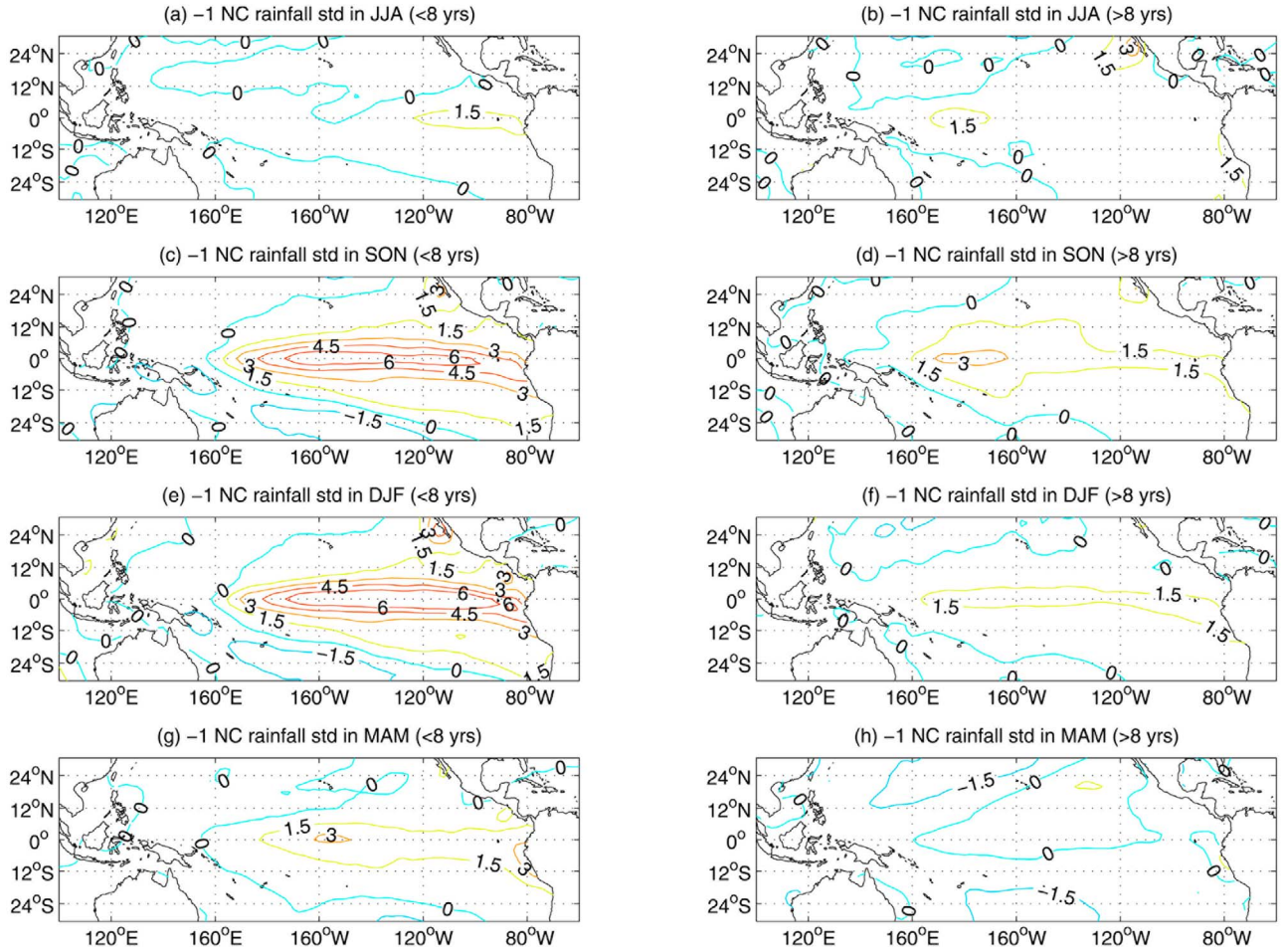

Figure 13. (a, b) June–August (JJA), (c, d) September–November (SON), (e, f) December–February (DJF), and (g, h) March–May (MAM) SSTAs (in 1/10th of °C) regressed onto NC rainfall in the (left) high (>1/8 cycle per year) and (right) low (<1/8 cycle per year) frequency. The displayed SSTAs are associated with −1 standard deviation of NC rainfall.

clearly stronger with CP indices (namely CP index, Niño 4 index, or EMI) rather than with EP ones. NC appears to be included in the core of the ENSO-related teleconnection pattern in the SW Pacific during the CP events in SON and DJF. Any paleoclimate record coming from NC [*Ourbak et al.*, 2006] should then mostly reflect CP events rather than EP ones.

[23] The EMI appears less optimal than Niño 4 SST or CP indices, because the negative rainfall anomalies, at least in SON, tend to be not significant at the 95% level for the upper 20% percentiles (e.g., warm events) EMI events. These results suggest that a simple ad hoc EMI poorly distinguishes impacts of CP events from impacts of EP events in NC and its use should be regarded with caution in other studies over the SW Pacific. This result is consistent with the study by *Taschetto et al.* [2009], who argued that the positive SSTAs around the dateline are the main driver of Australian monsoon variations and suggested that the cooling on both sides of the tropical Pacific that accompanies the central warming in Modoki signature [*Ashok et al.*, 2007] does not significantly affect the rainfall response. On the other hand, it should be noted that a given season could be simultaneously defined as a cold EP and a warm CP event and vice versa. For example, 1983 and 1998 are both a cold CP and a warm EP event and 1990 is a cold EP and a warm CP event in SON.

[24] The higher sensitivity of NC rainfall variations to CP events is first linked to the longitudinal match between NC and the location of the SSTAs during CP events. Second, although SSTAs are weaker in the central Pacific during CP events than in the east during EP ones, higher climatological SSTs around the dateline enable a strong positive feedback during the warm ENSO events through latent heat release in the middle and upper troposphere that significantly strengthens the southern Hadley cell around NC longitudes. The related anomalous subsidence leads to significant negative rainfall anomalies in the SW Pacific, including eastern Australia. These patterns are reversed and are even stronger during cold CP events.

[25] The atmospheric anomalies observed in SON and DJF are very dissimilar between warm CP and EP events and rather similar during the cold events with a larger magnitude during the CP events. This asymmetry is partly related to the superposition of the SSTAs to the annual cycle and the nonlinear sensitivity of atmospheric response to SSTAs near the dateline. The warm CP events in SON combine a large zonal SST gradient in the equatorial Pacific with the warmest

SST greater than 29.5 °C between 160°E and 180°E. This unique combination leads to an enhancement of the deep convection near the dateline in the equatorial Pacific and a strong subsidence in the SW Pacific, including NC. The zonal SST gradient weakens in DJF because of the annual warming of the equatorial east Pacific just before and after Christmas. The flattening of the zonal SST gradient in DJF tends to extend someway the meridional atmospheric response across a larger range of longitudes than in SON. The zonal SST gradient is weaker during warm EP events, while the associated SST are, by definition, colder in the sensitive longitudes near the dateline. In contrast, cold CP and EP events show a very strong zonal SST gradient with warmer SST in the warm pool (140°E–160°E) and a strong W–E gradient near the dateline during cold CP and EP events. The associated atmospheric anomalies are rather similar between both patterns, that is, an increased equatorial Walker circulation with the SPCZ shifted southwestward of its climatological location and an anomalous advection of moisture toward NC and most of the SW Pacific.

[26] Our study has demonstrated that the whole linear relationship between NC rainfall and ENSO from ASO to JFM comes from a superposition of two distinct bands, around 3–6 years and near 10–12 years. The superposition of both the bands is especially efficient in SON. The first band is related to the classical ENSO variability. This teleconnection peaks logically when ENSO strengthens around Christmas and is quasi-stationary from 1950 onward. The quasi-decadal teleconnection strengthens from ~1975 to 1980 onward and is strongest from AMJ to OND. The splitting of the ENSO teleconnection into two bands does not necessarily induce different mechanisms. The spatial structure of SST anomalies suggests that the quasi-decadal variability could be related to a large-scale phenomenon, which includes ENSO, or at least CP SST variations. *Power et al.* [1999] found a strong association between the magnitude of ENSO and all-Australia rainfall during the negative IPO phases, while the positive IPO phases showed a weaker relationship. The IPO, PDO, and Niño 4 SST indices in low frequency are inextricably linked to the warming and cooling of the tropical Pacific Ocean, but our results suggest that weak, but sustained, long-term warming of the central equatorial Pacific around the dateline, which seems especially large in SON, plays a role to explain the current strengthening of the linear relationship between NC rainfall and ENSO. This long-term trend is neither observed in IPO, which is defined from detrended and low-pass filtered SSTAs, nor in PDO. The real pattern of this long-term trend remains to be established, but we can hypothesize that it is larger in the Southern Hemisphere and/or tropics. Understanding the long-term trend is necessary for the success of seasonal prediction of any impact from the ENSO phenomenon, such as fire occurrence at the end of the dry season during recent years [*Barbero et al.*, 2011].

[27] **Acknowledgments.** This study is funded by a grant from ANR under the INC program (grant ANR-07-BDIV-008). The meteorological data are extracted from the Météo-France database with the kind help of Y. Bidet (Météo-France, Aix-en-Provence) and Y. Noack (CEREGE). We also thank *Grinsted et al.* [2004] for developing the wavelet toolbox available at http://www.pol.ac.uk/home/research/waveletcoherence/, H.F. Graf, M. Fischer, and an anonymous reviewer whose positive comments improved our article. Finally, we thank Amanda Cherruy who read our revised draft and significantly improved it.

References

Ashok, K., S. K. Behera, S. A. Rao, H. Weng, and T. Yamagata (2007), El Niño Modoki and its possible teleconnections, *J. Geophys. Res.*, *112*, C11007, doi:10.1029/2006JC003798.

Barbero, R., V. Moron, M. Mangeas, M. Despinoy, and C. Hély (2011), Relationships between MODIS and ATSR fire and atmospheric variability over New Caledonia (SW Pacific), *J. Geophys. Res.*, *116*, D21110, doi:10.1029/2011JD015915.

Chao, Y., M. Ghil, and J. C. McWilliams (2000), Pacific interdecadal variability in this century's sea surface temperature, *Geophys. Res. Lett.*, *27*, 2261–2264, doi:10.1029/1999GL011324.

Compo, G. P., et al. (2011), The Twentieth Century Reanalysis Project, *Q. J. R. Meteorol. Soc.*, *137*, 1–28, doi:10.1002/qj.776.

Feng, J., L. Wang, W. Chen, S. K. Fong, and K. C. Leong (2010a), Different impacts of two types of Pacific Ocean warming on Southeast Asian rainfall during boreal winter, *J. Geophys. Res.*, *115*, D24122, doi:10.1029/2010JD014761.

Feng, J., W. Chen, C.-Y. Tam, and W. Zhou (2010b), Different impacts of El Niño and El Niño Modoki on China rainfall in the decaying phases, *Int. J. Climatol.*, *31*, 2091–2101, doi:10.1002/joc.2217.

Fischer, M., B. Dewitte, and L. Maîtrepierre (2004), A non-linear statistical downscaling model: El Niño/Southern Oscillation impact on precipitation over New Caledonia, *Geophys. Res. Lett.*, *31*, L16204, doi:10.1029/2004GL020112.

Folland, C. K., J. A. Renwick, M. J. Salinger, and A. B. Mullan (2002), Relative influences of the interdecadal Pacific oscillation and ENSO on the South Pacific convergence zone, *Geophys. Res. Lett.*, *29*(13), 1643, doi:10.1029/2001GL014201.

Gaucherel, C. (2009), Analysis of ENSO interannual oscillations using nonstationary quasi-periodic statistics: A study of ENSO memory, *Int. J. Climatol.*, *30*, 926–934.

Gillett, N. P., T. D. Kell, and P. D. Jones (2006), Regional climate impacts of the Southern Annular Mode, *Geophys. Res. Lett.*, *33*, L23704, doi:10.1029/2006GL027721.

Grinsted, A., J. C. Moore, and S. Jevrejeva (2004), Application of the cross wavelet transform and wavelet coherence to geophysical time series, *Nonlinear Processes Geophys.*, *11*, 561–566, doi:10.5194/npg-11-561-2004.

Guilderson, T. P., and D. P. Schrag (1998), Abrupt shift in subsurface temperatures in the tropical Pacific associated with changes in El-Niño, *Science*, *281*, 240–243, doi:10.1126/science.281.5374.240.

Hill, K. J., A. S. Taschetto, and M. H. England (2009), South American rainfall impacts associated with inter-El Niño variations, *Geophys. Res. Lett.*, *36*, L19702, doi:10.1029/2009GL040164.

Janicot, S., V. Moron, and B. Fontaine (1996), Sahel droughts and ENSO dynamics, *Geophys. Res. Lett.*, *23*, 515–518, doi:10.1029/96GL00246.

Kalnay, E., et al. (1996), The NCEP/NCAR 40-Year Reanalysis Project, *Bull. Am. Meteorol. Soc.*, *77*, 437–471, doi:10.1175/1520-0477(1996)077<0437:TNYRP>2.0.CO;2.

Kao, H. Y., and J.-Y. Yu (2009), Contrasting eastern-Pacific and central-Pacific types of ENSO, *J. Clim.*, *22*, 615–632, doi:10.1175/2008JCLI2309.1.

Katz, R. W., and M. H. Glantz (1986), Anatomy of a rainfall index, *Mon. Weather Rev.*, *114*, 764–771, doi:10.1175/1520-0493(1986)114<0764:AOARI>2.0.CO;2.

Lefèvre, J., P. Marchesiello, N. Jourdain, C. Menkes, and A. Leroy (2010), Weather regimes and orographic circulation around New Caledonia, *Mar. Pollut. Bull.*, *61*, 413–431, doi:10.1016/j.marpolbul.2010.06.012.

Mantua, N. J., S. R. Hare, Y. Zhang, J. M. Wallace, and R. C. Francis (1997), A Pacific interdecadal climate oscillation with impacts on salmon production, *Bull. Am. Meteorol. Soc.*, *78*, 1069–1079, doi:10.1175/1520-0477(1997)078<1069:APICOW>2.0.CO;2.

Micevski, T., S. W. Franks, and G. Kuczera (2005), Multidecadal variability in coastal eastern Australian flood data, *J. Hydrol.*, *327*, 219–225, doi:10.1016/j.jhydrol.2005.11.017.

Morlière, A., and J. P. Rébert (1986), Rainfall shortage and El Niño Southern Oscillation in New Caledonia, Southwestern Pacific, *Mon. Weather Rev.*, *114*, 1131–1137, doi:10.1175/1520-0493(1986)114<1131:RSAENO>2.0.CO;2.

Moron, V., A. W. Robertson, M. N. Ward, and P. Camberlin (2007), Spatial coherence of tropical rainfall at the regional scale, *J. Clim.*, *20*, 5244–5263, doi:10.1175/2007JCLI1623.1.

Nicet, J.-B., and T. Delcroix (2000), ENSO-related precipitation changes in New Caledonia, Southern tropical Pacific: 1969–98, *Mon. Weather Rev.*, *128*, 3001–3006, doi:10.1175/1520-0493(2000)128<3001:ERPCIN>2.0.CO;2.

Ourbak, T., T. Correge, B. Malaize, F. Le Cornec, K. Charlier, and J. P. Peypouquet (2006), ENSO and interdecadal climate variability over the last century documented by geochemical records of two coral cores from

the South West Pacific, *Adv. Geosci.*, *6*, 23–27, doi:10.5194/adgeo-6-23-2006.

Power, S., T. Casey, C. Folland, A. Colman, and V. Mehta (1999), Inter-decadal modulation of the impact of ENSO on Australia, *Clim. Dyn.*, *15*, 319–324, doi:10.1007/s003820050284.

Power, S., M. Haylock, R. Colman, and X. Wang (2006), The predictability of interdecadal changes in ENSO activity and ENSO teleconnections, *J. Clim.*, *19*, 4755–4771, doi:10.1175/JCLI3868.1.

Salinger, M. J., R. E. Basher, B. B. Fitzharris, J. E. Hay, P. D. Jones, J. P. Macveigh, and I. Schmidely-Leleu (1995), Climate trends in the South-West Pacific, *Int. J. Clim.*, *15*, 285–302, doi:10.1002/joc.3370150305.

Smith, T. M., R. W. Reynolds, T. C. Peterson, and J. Lawrimore (2008), Improvements to NOAA's historical merged land-ocean surface temperature analysis (1880–2006), *J. Clim.*, *21*, 2283–2296, doi:10.1175/2007JCLI2100.1.

Taschetto, A. S., and M. H. England (2009), El Niño Modoki impacts on Australian rainfall, *J. Clim.*, *22*, 3167–3174, doi:10.1175/2008JCLI2589.1.

Taschetto, A. S., C. C. Ummenhofer, A. Sen Gupta, and M. H. England (2009), Effect of anomalous warming in the central Pacific on the Australian monsoon, *Geophys. Res. Lett.*, *36*, L12704, doi:10.1029/2009GL038416.

Trenberth, K. E., and D. P. Stepaniak (2001), Indices of El-Niño evolution, *J. Clim.*, *14*, 1697–1701, doi:10.1175/1520-0442(2001)014<1697:LIOENO>2.0.CO;2.

Vincent, D. G. (1994), The South Pacific Convergence Zone (SPCZ): A review, *Mon. Weather Rev.*, *122*, 1949–1970, doi:10.1175/1520-0493(1994)122<1949:TSPCZA>2.0.CO;2.

Vincent, E. M., M. Lengaigne, C. E. Menkes, N. C. Jourdain, P. Marchesiello, and G. Madec (2009), Interannual variability of the South Pacific Convergence Zone and implications for tropical cyclone genesis, *Clim. Dyn.*, *36*, 1–16, doi:10.1007/s00382–009–0716–3.

Wang, G., and H. Hendon (2007), Sensitivity of Australian rainfall to inter-El-Niño variations, *J. Clim.*, *20*, 4211–4226, doi:10.1175/JCLI4228.1.

Weng, H., K. Ashok, S. Behera, S. A. Rao, and T. Yamagata (2007), Impacts of recent El Niño Modoki on dry/wet conditions in the Pacific rim during boreal summer, *Clim. Dyn.*, *29*, 113–129, doi:10.1007/s00382-007-0234-0.

Xie, P., and P. A. Arkin (1996), Analyses of global monthly precipitation using gauge observations, satellite estimates and numerical model predictions, *J. Clim.*, *9*, 840–858, doi:10.1175/1520-0442(1996)009<0840:AOGMPU>2.0.CO;2.

Zhang, Y., J. M. Wallace, and D. S. Battisti (1997), ENSO-like interdecadal variability: 1900–93, *J. Clim.*, *10*, 1004–1020, doi:10.1175/1520-0442(1997)010<1004:ELIV>2.0.CO;2.

R. Barbero and V. Moron, Université d'Aix-Marseille, CEREGE, UMR 6635, Europôle de l'Arbois, BP80, F-13545 Aix-en-Provence CEDEX 04, France. (barbero@cerege.fr)